Numerical experiments in glacial inceptions in Northern Europe

ESPELETA BOLIVAR, Ruben Dario

Research project
Presented in partial fulfillment of the requirements for the degree of
Master applied mechanics

Universitè Grenoble Alpes
April 19, 2023

Project advisor(s):
Ph.D. Dr. Cruz Molina Garcia

Contents

1 Introduction

Ice sheets are important components of global climate systems [Zhang et al., 2017]. The impacts of the perturbation of these climate systems are most acutely changes in global sea level, as ice sheets grow or decay in response to climate forcing and internally controlled dynamics. While the rate of present-day sea-level rise is dominated by ocean steric changes and eustatic changes due to shrinking mountain glaciers, the eustatic contribution from the large ice sheets (Greenland and Antarctic) has increased in recent decades and it is expected to continue increasing in coming decades and centuries [Clark et al., 2015]. To have a better idea, if all the ice were to melt completely, the sea level would rise by an estimated 65m [Morlighem et al., 2017, Haywood et al., 2011] and force populations to emigrate their land submerged by water.

In order to understand these impacts on the dynamics and melting of ice sheets and glaciers, numerical models are developed. Through these models, some of them which are based on finite elements, we can have simulations that can make better predictions of future ice sheets' behavior and rate of sea level rise, and ultimately provide policymakers with improved estimates of future change.

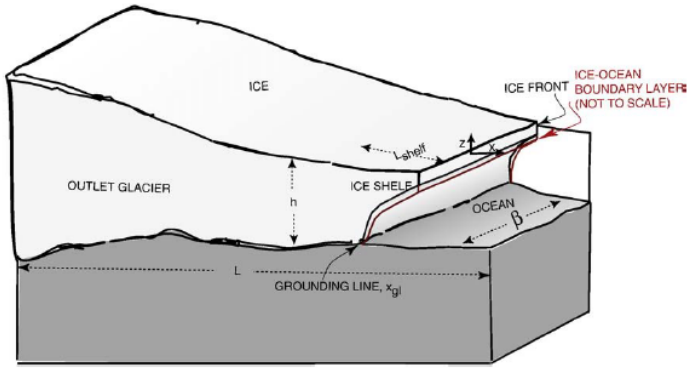

Figure 1: Schematic simplified diagram of the model domain of a glacier [Parizek and Walker, 2010]

There are different variables that play an important role in the dynamics of the glaciers. There is, for example, the grounding line. Its location is still a topic of discussion in the literature surrounding ice sheet dynamics [Goldberg et al., 2018].

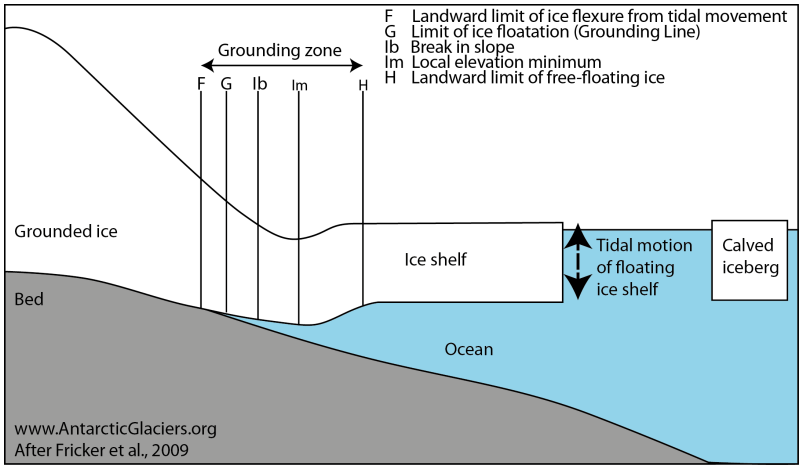

Figure 2: Schematic of a tributary glacier where we can observe the different parts denoting the grounding zone [Fricker et al., 2009].

Glaciers that end in the ocean are called tidewater glaciers. Glaciers that flow into an ice shelf are called tributary glaciers as the one shown in figure 1 by [Parizek and Walker, 2010]. The line

that divides the part of the glacier that is in contact with the solid bedrock and the ice shelf floating on water driven by buoyancy, is called the grounding line [Cheng et al., 2019]. The location of the grounding line is important because the mass loss from glaciers is strongly linked to changes in the ice shelves and their grounding lines [Brunt et al., 2010, Pritchard et al., 2012]. Its long-term horizontal position is very susceptible to temporal and spatial changes in ice thickness and sea level, as well as bedrock and ice surface slopes. Ice thinning and rising sea levels can cause grounding lines to retreat while thickening or declining sea levels can cause an advance [Friedl et al., 2020]. It is important to know the grounding line position to be able to quantify the ice discharge into the sea and as an indicator, if the ice sheet is advancing or retreating [Konrad et al., 2018].

Grounding lines are actually more of a zone. The grounding zone is the region where ice transitions from a grounded ice sheet to a freely floating ice shelf, typically over several kilometers. The grounding zone is the region between point F in figure 2 by [Fricker et al., 2009], where there is no tidal movement, and point H, which is the seaward limit of ice flexure, where the ice is free-floating. The floating ice shelf changes in elevation in response to tides, atmospheric air, pressure, and oceanic processes. Grounding occurs when the ice shelf comes into contact with the bedrock below [Fricker et al., 2009]. The transition from grounded ice sheets to floating ice shelves plays an important role in controlling marine ice sheet dynamics, as it determines the rate at which ice flows out of the grounded part of the ice sheet [Schoof, 2007a]. This is because ice flux through the grounding line increases sharply with ice thickness at the grounding line. This means that grounding lines are unstable on reverse-bed slopes, such as those under Pine island glaciers, because recession into deeper water increases ice flux and further encourages more glacier recession [Schoof, 2007b].

This project aims to understand the direct impact of changes in the position of the grounding line on the flow dynamics of ice sheets glaciers. We will use the finite element model Elmer/Ice to explore the spatial resolution impact on the grounding line position. We will compare the changes in the position of the grounding line for two different idealized topographies. This will let us understand the behavior of real present and past glaciers such as the Northern European glacier.

2 Glacier dynamics

2.1 Mass and movement balance equations

An ice sheet is a continuous sheet of land ice that covers a very large area of several thousand to millions of square meters. It is formed by an accumulation of snow which will densify under its own weight until it becomes ice. This ice will then flow downhill under its weight, and can eventually reach the sea. If it does, and the ice propagates above the sea, this part of the ice sheet is called an ice shelf [Hutter, 1982]. Figure 1 shows a diagram of an ice sheet showing different parts of it, such as the ice shelf, and some phenomena happening inside of it, such as the ice flow or the snow accumulation.

For large time scales the ice is considered a very viscous fluid. The ice flow equations are then derived from the Stokes equation [Hutter, 1982]:

$$div\sigma + \rho g = div\tau - gradp + \rho g = 0; \tag{1}$$

with σ the stress tensor, ρ the density of the ice, g the gravity vector, τ the deviatoric stress tensor, with $\sigma = \tau - pI$ and $p = \frac{tr\sigma}{3}$.

And the mass conservation:

$$\frac{dh}{dt} + div(uH) = M_s + M_b; \tag{2}$$

With u the velocity, H the ice thickness, M_s and M_b the mass balance at the surface and at the bottom respectively. M_s will be defined, and M_b is considered as 0 for convenience purposes.

The stresses are related to the viscosity and the strain by Glen's law [Glen, 1958]:

$$\tau = 2\eta\dot{\epsilon}, \tag{3}$$

with the viscosity given by:

$$\eta = \frac{1}{2}(EA)^{\frac{-1}{n}} \dot{\epsilon_e}^{\frac{(1-n)}{n}}. \tag{4}$$

Where:

- The strain rate $\dot{\epsilon}$.
- Glen's constant n=3.
- The enhancement factor to account for an anisotropic effect E=1.
- The rheological parameter A=15,46.

For an ice sheet, the ratio of the vertical length over the horizontal length is more than $1 : 10^3$. Indeed, the thickness of an ice sheet goes from 0 m to a few thousand of meters (e.g. the ice sheet in Greenland is 3300 m thick at most [Bamber et al., 2001,]) and the typical horizontal length of an ice sheet is of the order of magnitude of 1000 km. This allows us to apply the shallow ice approximation. It assumes a large ratio of horizontal to vertical length, that the basal shear stress is balanced by the gravitational driving stress, and a large vertical to horizontal stress ratio. That represents a slow flow in the interior of an ice sheet (blue regions in Figure 3). The approximation makes the method computationally cheaper than the Full-Stokes model with good accuracy over long simulations.

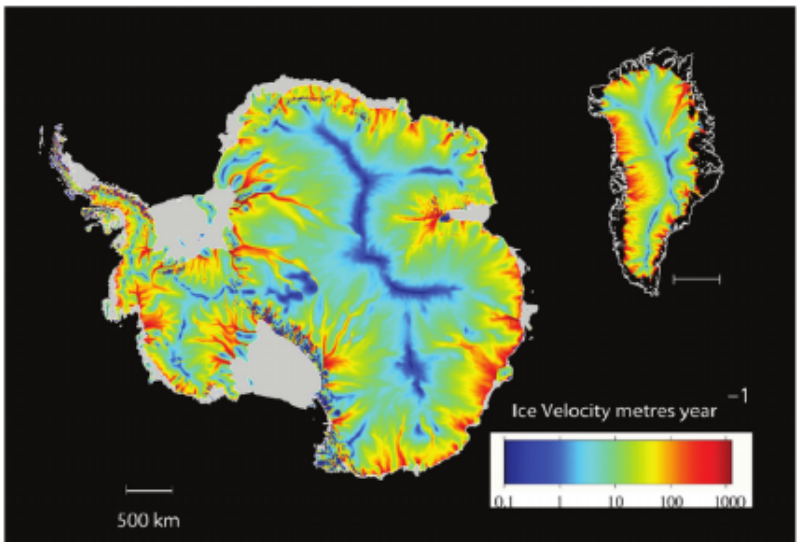

Figure 3: Ice velocities in Antarctica and Greenland topographies, where we can see in red the highest velocity profiles in the glaciers and as a consequence we consider the basal shear stress as 0 and the longitudinal stress dominates, which allows using a Shallow Shelf approximation [Allison et al., 2009,].

Figure 3 shows a map of velocities in Antarctica and Greenland topographies. Where this velocity is the highest, the basal shear stress cannot be considered balanced by gravity anymore. Instead, it is taken as 0 and the longitudinal stress dominates. This is the Shallow Shelf approximation, initially developed for ice shelves, but which has been extended to dragging ice streams. It is a 2D vertically integrated model, the ice velocity being depth-averaged.

But these approximations are not mandatory: the Full Stokes model is still the most precise, it accounts for all nine stress components. It is useful around the parts that are at the limits of the other models or over complex topographies, but not needed for the interior of ice sheets, where the improvement would be minimal but the computational cost way higher [Larour et al., 2012].

The factors such as sensitivity, long time intervals, and long distances require careful treatment of the groundline neighborhood by the numerical method to discretize the model equations [Cheng et al., 2019]. The most accurate ice model is the Full Stokes (FS) equations [Cheng et al., 2019].

However, a simplification of these FS equations by integrating into the depth of the ice is the shallow shelf approximation [MacAyeal, 1989]. The computational advantage with Shallow Shelf approximation is that the dimension of the problem is reduced by one, it is often used for simulations of the interaction between a grounded ice sheet and a marine ice shelf [Cheng et al., 2019]. In this project, only the Shallow Shelf approximation is made, as this is how future projections of Greenland and Antarctica are done with the Elmer/Ice model.

2.2 Grounding line stability

A long debate on the dynamics of such ice sheets was initiated in the 1970s when [Weertman, 1974] proposed that a marine ice sheet that lies on an upward-sloping bed is unstable. Recently, the instability hypothesis has been strongly reinforced, based on a boundary-layer theory due to [Schoof, 2007a]. Moreover, [Vieli and Payne, 2005] showed the poor ability of marine ice-sheet models to give consistent prognostic results and, more particularly, they highlighted the influence of the grid size on model results. One of their main conclusions was that no reliable model was able to predict grounding line dynamics at the time of their study.

There is a need to improve marine ice-sheets models in order to corroborate recent theoretical predictions and to obtain confident simulations of the grounding line dynamics. [Durand et al., 2009a] proposed a full-Stokes solution of the ice-sheet/ice-shelf transition. This approach has been built on literature dealing with the coupling between a grounded ice sheet and a floating ice shelf and identifying this transition zone as a crucial control of the marine ice sheet dynamics [Weertman, 1974, Van der Veen, 1985, Chugunov and Wilchinsky, 1996, Hindmarsh, 1996, Vieli and Payne, 2005, Schoof, 2007a, Schoof, 2007b,].

[Durand et al., 2009b] showed, using the finite element code Elmer/Ice, that the full-Stokes modeling of the ice-sheet/ice-shelf transition gives a consistent prediction of grounding-line migration. However, their approach is highly sensitive to the chosen mesh resolution. For a grid size smaller than $5km$ in the grounding-line vicinity, predictions start to be consistent. For any finer resolution than $5km$, the steady-state grounding-line position is the same (6km is the standard deviation). If a sub-grid refinement of 200m in the vicinity of the grounding line is applied the steady-state position is stable.

In order to study and test the behavior of the different components of the models, idealized systems are studied and, based on the results that are obtained from these idealized cases, the hypothesis, models, and numerical methods used to solve the problems are improved. For this reason, within the framework of this project, we will analyze the behavior of the Elmer/Ice method to solve idealized systems and topographies. The framework in which the present project is focused is on the study of the Northern Europe glacier. But, since this glacier does not exist anymore, idealized cases simulations of North Europe glaciers, such as Greenland can be analyzed as mentioned before, and their results can be used to improve the numerical models, hypothesis, and parameters of the models, and this way we can better understand the behavior of ancient glaciers such as the Northern Europe glacier.

3 Numerical model

3.1 The Elmer/Ice finite element method

Most of the time analytical solutions are challenging or even impossible to obtain. In order to model ice sheets, both the finite difference method (FDM) and the finite element method (FEM) are used. The finite difference method consists in converting ordinary and partial differential equations into a system of linear equations by approximating derivatives as finite differences. Elmer/Ice, on the other hand, uses the finite element method. The ice sheet/ice flow model Elmer/Ice includes developments related to glaciological problems and a large number of dedicated solvers and user functions that solve the Full-Stokes equations for various ice rheologies (classical, Glenn's flow law, anisotropic laws, and porous compressible firns/snow law). It includes solvers for the classical asymptotical expansions of the Stokes equations, namely the shallow ice approximation and the shallow and shallow shelf approximation (SSA). All these equations can be solved diagnostically or transiently, allowing the displacement of the boundaries.

Elmer/Ice considers a continuum as an assembly of non-overlapping elements forming the same geometry, which makes the modeling of complex geometries possible. Each element is made of at least two points, which are applied to the forces and computed the displacements. To solve the equations, Elmer/Ice uses subroutines or solvers. Each equation corresponds to one solver to be referenced in the input file, together with the different parameters of the problem. They each compute the evolution of given variables, such as the ice thickness or the velocity, to give at each time step a picture of the flow. All combined, it allows us to visualize the evolution of the flow through time.

Here I can put the figures showing the mesh for a quarter domain for thule and the cone.

3.2 Tophographic profiles

This numerical experiment uses two different topographic profiles. A cone and a more realistic topography (Thule).

3.2.1 Cone

The idealized model consists of a circular bedrock configuration (Figure 4) given by:

$$\theta = arctan2(y, x); \tag{5}$$

$$I = R - cos(2\theta)\frac{R}{2} \tag{6}$$

$$Bed_0 = Bc - (Bc - BI)\frac{|x^2 + y^2|}{R2}; \tag{7}$$

Where $R = 800x10^3m$, $Bc = 0.9x10^3m$, and $BI = -2x10^3m$.

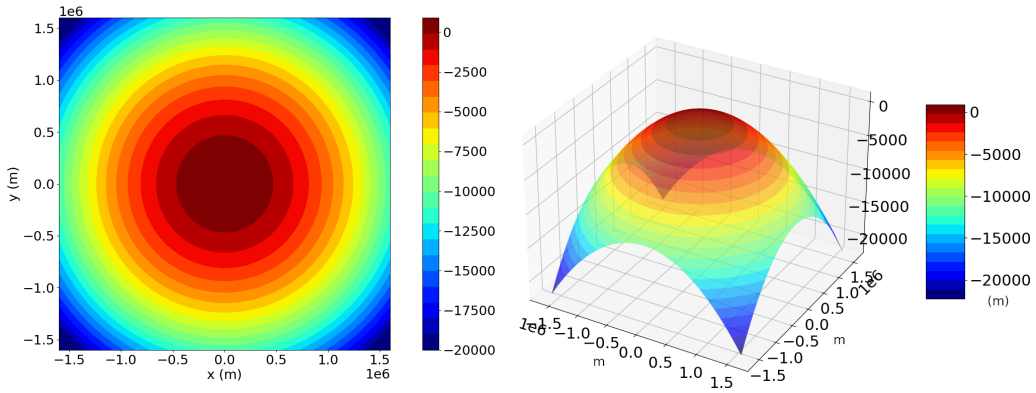

Figure 4: Circular bedrock topography. On the left side top view and on the right side, lateral view.

3.2.2 Thule

The Thule bedrock configuration is shown in Figure 5 and 6 and is given by:

$$\theta = arctan2(y, x); \tag{8}$$

$$I = R - cos(2\theta)\frac{R}{2}; \tag{9}$$

$$Bed_0 = Bc - (Bc - BI)\frac{|x^2 + y^2}{R^2}; \tag{10}$$

$$Bed = Bacos(3\pi\frac{\sqrt[2]{x^2 + y^2}}{I}) + Bed_0; \tag{11}$$

With $R = 800x10^3m$, $Bc = 0,9x10^3m$, $BI = -2x10^3m$, and $Ba = 1,1x10^3$.

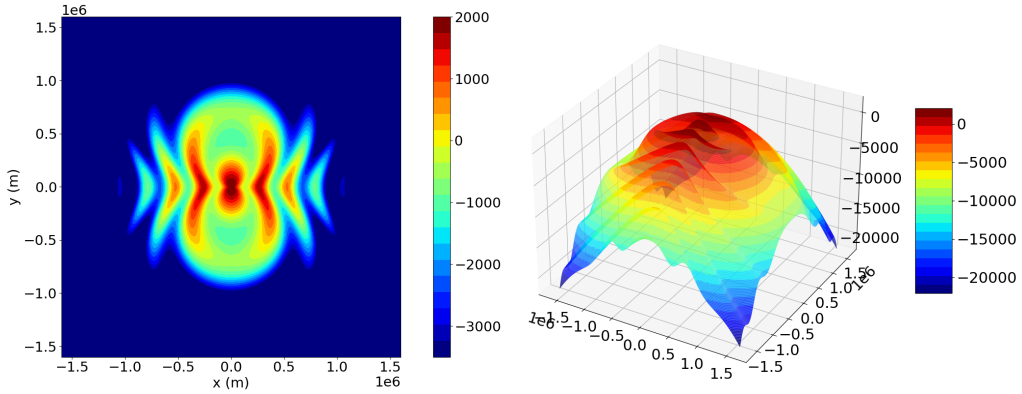

Figure 5: Thule bedrock topography 3D. On the left side the top view, and on the right side a lateral view.

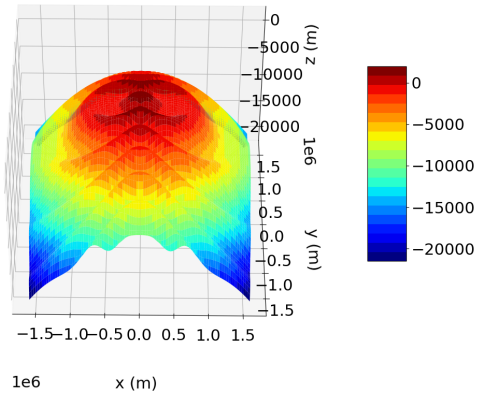

Figure 6: Thule bedrock topography 3D with a front view.

3.3 Boundary conditions

Boundary conditions are needed in order to solve differential equations. It will be assumed that:

- The bedrock is impermeable (The vertical component of the ice flow velocity is 0).
- The flow follows the Weertman friction law.
- Mass accumulation is a constant parameter.
- The simulation will be performed on a quarter of the domain since the geometry of the topography is symmetric, which allows having free slip boundary conditions at the left and downsides of the topography, and open boundary conditions at the right and top sides of the domain.

3.4 Physical constants

Table 1shows the constants parameters that were set up for the experiment by the Calvin MIP project at the beginning of the project.

After modifications were done in the experiment proposal, the final values used in the simulations are the ones listed in Table 2

For the computation of $u_b = 2$, we used the Weertman style sliding law:

$$u_b = C\tau_b^m \tag{12}$$

Table 1: Physical constants 1

Variable	Description	Units
$g = 9.81$	Gravitational acceleration	ms^{-2}
$a_s = 0.3$	Surface mass balance (SMB)	ma^{-1}
$a_b = 0$	Basal mass balance (BMB)	ma^{-1}
$\rho i = 917$	Ice density	kgm^{-3}
$\rho w = 1030$	Sea water density	kgm^{-3}
$A = 2.9377x10^{-9}$	Ice rate factor	$KPa^{-3}a^{-1}$
$n = 3$	Flow law stress exponent	
$C = 0.001$	basal slipperiness	$ma^{-1}Kpa^{-3}$
$m = 3$	Sliding law stress exponent	
$d2a = 365.2422$	days in a year	days

Table 2: Physical constants

Variable	Description	Units
$g = 9.81$	Gravitational acceleration	ms^{-2}
$a_s = 0.3$	Surface mass balance (SMB)	ma^{-1}
$a_b = 0$	Basal mass balance (BMB)	ma^{-1}
$\rho i = 917$	Ice density	kgm^{-3}
$\rho w = 1028$	Sea water density	kgm^{-3}
$A = 2.9377x10^{-9}$	Ice rate factor	$KPa^{-3}a^{-1}$
$n = 3$	Flow law stress exponent	
$C = 0.001$	basal slipperiness	$ma^{-1}Kpa^{-3}$
$m = 3$	Sliding law stress exponent	
$s2a = 31556926$	Seconds in a year	seconds

where C is the basal slipperiness and τ_b is the basal shear stress. In order to enter these values into the Elmer code, we need to convert all units to Elmer units, namely: MPa, meter, and years. It means that all units that are derivated from time in seconds, must be converted to time in years using the time equivalence proposed in the project and all units or values expressed in terms of KPa must be multiplied by a factor of 10^{-3} to be converted to MPa. Also, to compute the basal sliding velocity u_b, Elmer uses the term β that is related to u_b by:

$$\tau = \beta u_b^{\frac{1}{m}} \tag{13}$$

So, we have:

$$u_b = (\frac{\tau}{\beta})^m; \tag{14}$$

$$u_b = \frac{1}{\beta^m}\tau^m \tag{15}$$

Using the notation from equation (1), we can say that $C = \frac{1}{\beta^m}$. So, we can compute β as:

$$\beta = (\frac{1}{C})^{\frac{1}{3}} \tag{16}$$

If we replace C by its value given in table 2, we get $\beta = 10^4 Pam^{\frac{-1}{3}} a^{\frac{1}{3}}$ which converted to Mpa will give us a value of 10.

3.4.1 Numerical parameters

The numerical resolution will be our variable physical parameter, which we will vary from 10 km, 5 km, 2 km, 1 km, 500 m, and 250 m.

3.4.2 External forcing

We will assume that the only external force acting is gravity ($g = 9.81m/s^2$), which is translated to the weight of the ice sheet and the flotation force of this in the ocean water.

3.4.3 Initial condition

The simulation departs from no iced configuration. As stated before, the flow will follow the linear Weertman friction law at the base of the ice sheet:

$$\tau_b = \beta u; \tag{17}$$

Where τ is the friction shear stress, β is the basal friction coefficient, and u is the velocity. Comparisons were made using friction coefficients ranging from $\beta = 10^{-8}$ to simulate a friction close to 0, to $\beta = 10^{-2}$. This coefficient is also the one chosen to perform the simulations.

3.4.4 Time step

The Courant-Friedrichs-Lewy (CFL) condition is a necessary condition to solve numerical partial differential equations. It states that the distance a variable travels between two-time steps must be smaller than the distance between two points of the mesh [Courant et al., 1967,]. It is needed that:

$$C = \frac{u\Delta t}{\Delta x} < Cmax; \tag{18}$$

With C the courant number, u the magnitude of the velocity, Δt the time step, Δx the horizontal resolution, and Cmax = 1. This implies then, for a given mesh:

$$\Delta t < \frac{\Delta x}{u}; \tag{19}$$

This is a safe approximation. Cmax then has to be estimated by running different parameters in the simulation and seeing if it converges or not. In order to satisfy the CFL condition, a good starting point is 1 year, since it works properly and converges even for a resolution of 1km. However, in this experiment, it is asked to report the results every 10 years, and for this reason, we will save the results of the simulation with a frequency of 10 years.

4 Results

As mentioned before, the simulations using Elmer/Ice use unstructured meshes, as shown in the left-hand side of figure 7 for a 10km resolution mesh. This is very helpful in terms of simulating complex geometries, for example, the thule configuration.

However, once the simulation is done and to better interpret the results obtained, we need to build a structured mesh, because it is ideal for these time-domain simulations this way we can easily identify elements and nodes when plotting time-dependent or spacial-dependent graphics. In our case, our objective of interest will be the spacial behavior or dynamic of the glacier since we will analyze the position of the grounding line after the steady state is reached. To build the structured mesh, we performed an interpolation made from the unstructured mesh values of the nodes, namely we interpolate per each node the value of the variables of interest with the values of these variables in the non-structured mesh. This way we know which position the node is in, and we can plot figures spacial-dependent, namely, we can plot the value of different variables, for example, the velocity components, as a function of the horizontal position.

4.1 Cone configuration

Figure 9 shows a snap of the final steady state result of the simulation for the computation of two of the variables, namely the thickness and thickness velocity (or thickness rate change) of the ice sheet with the 10km mesh resolution, in figure 9a and 9b, respectively. It can be observed that the

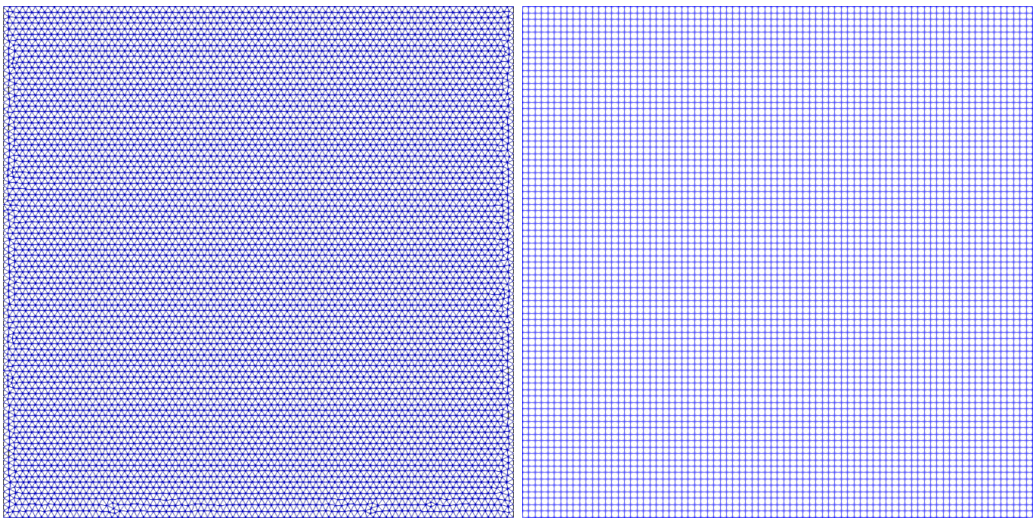

Figure 7: a) 10km resolution non-structured mesh used in Elmer/Ice. b) Regular structured mesh for 10km resolution.

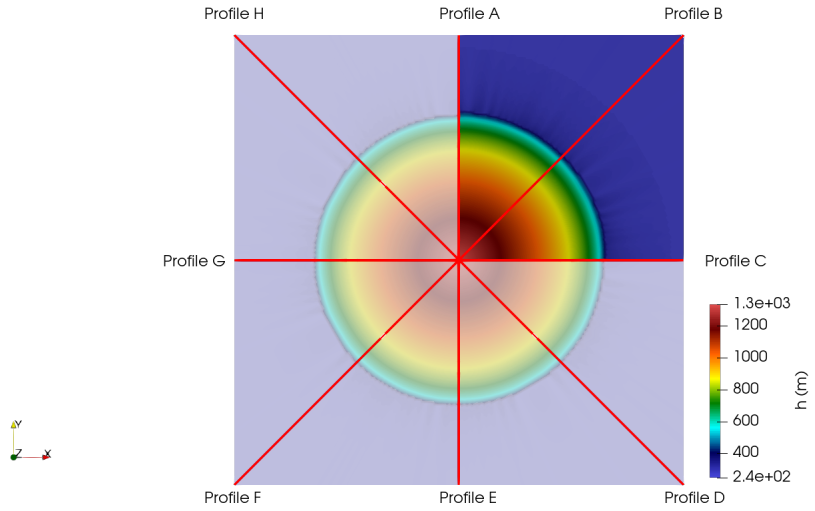

Figure 8: Circular domain experimental profiles proposed for cone configuration. Highlighted the quarter of the domain.

final rate change for the ice thickness varies within a range of very small values in all the domain, and for this reason, we conclude the convergence of the simulation.

For this configuration, the simulations were done using different resolutions with the same parameters listed in table 2. Figure 12 shows the first simulation made for this resolution, and the result shown is the thickness of the ice sheet, as a function of the horizontal distance. We see in red the position of the bedrock, so this way the result shows that the zone where the lower part of the glacier (green) separates from the bedrock, corresponds to the grounding line position, at the steady state after 10,000 thousand years of simulation.

Figure 13 shows a comparison of the position of the grounding line for different mesh resolutions, starting from 10km until 1km. We see how the differences in position start to decrease as we decrease the mesh resolution.

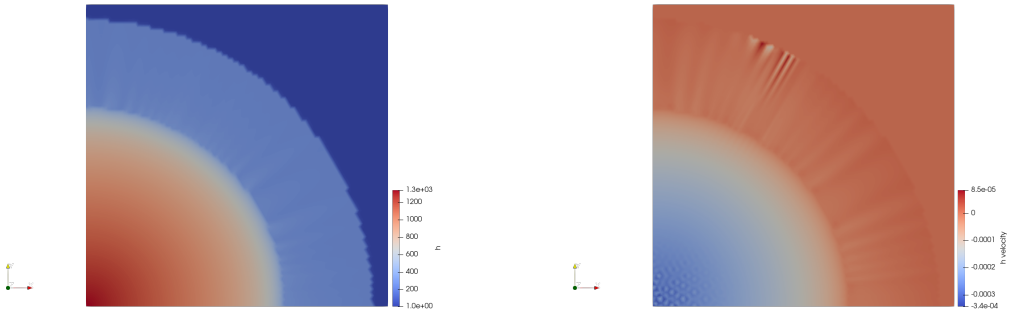

(a) Thickness of the ice denoted as h.

(b) Ice thickness velocity in the domain.

Figure 9: Plots of the ice sheet thickness and the ice thickness velocity at the steady state for 10km resolution mesh.

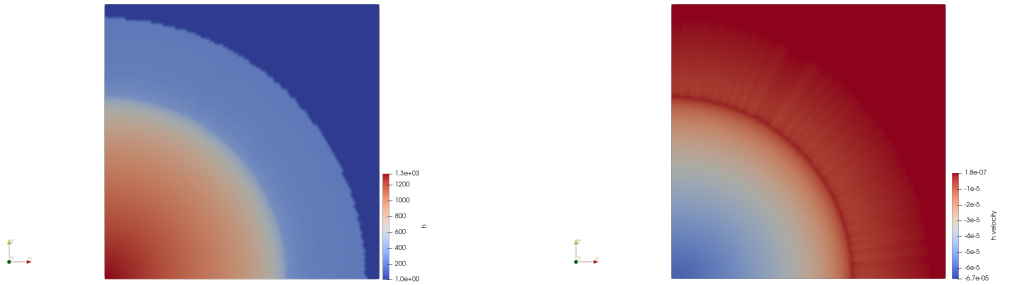

(a) Thickness of the ice denoted as h.

(b) Ice thickness velocity in the domain.

Figure 10: Plots of the ice sheet thickness and the ice thickness velocity at the steady state for 5km resolution mesh.

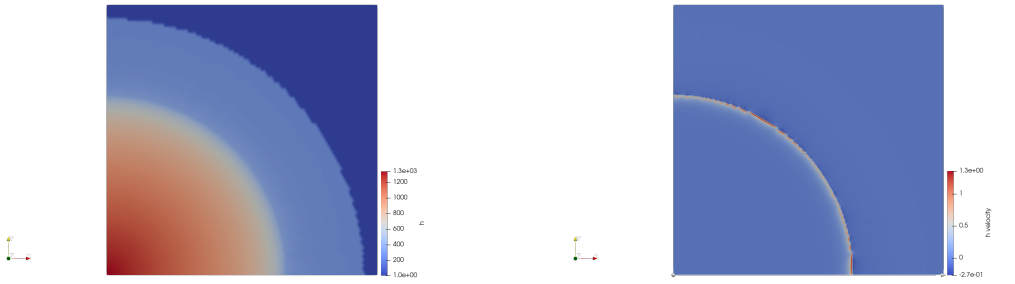

(a) Thickness of the ice denoted as h.

(b) Ice thickness velocity in the domain.

Figure 11: Plots of the ice sheet thickness and the ice thickness velocity at the steady state for 2km resolution mesh.

4.2 Thule configuration

For the second part of the experiments, the results for the thule configuration were obtained for a quarter of the domain, and following the Calving MIP intercomparison project, the graphs of the variables as a function of the position were plot along the two profiles proposed, namely Halbrane B and Caprona B as shown in figure **??**.

For the results after the steady state is reached, figure 16 shows the heights zb and zs along the Caprona B profile, for the 10km resolution (figure 16a) and 5km resolution (figure 16b).

The same procedure was performed along the Halbrane B line, which results are summarized

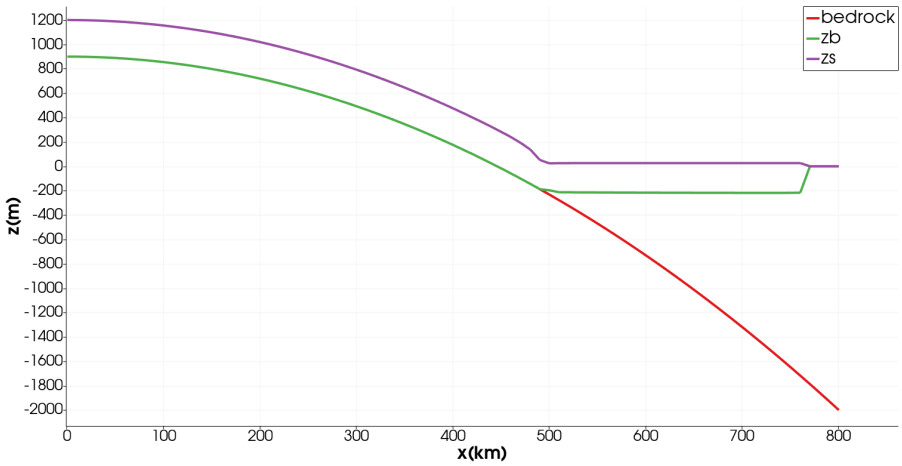

Figure 12: Height of the upper and down part of the ice sheet, denoted as zb and zs, respectively, for a 10km resolution mesh using a quarter of the domain.

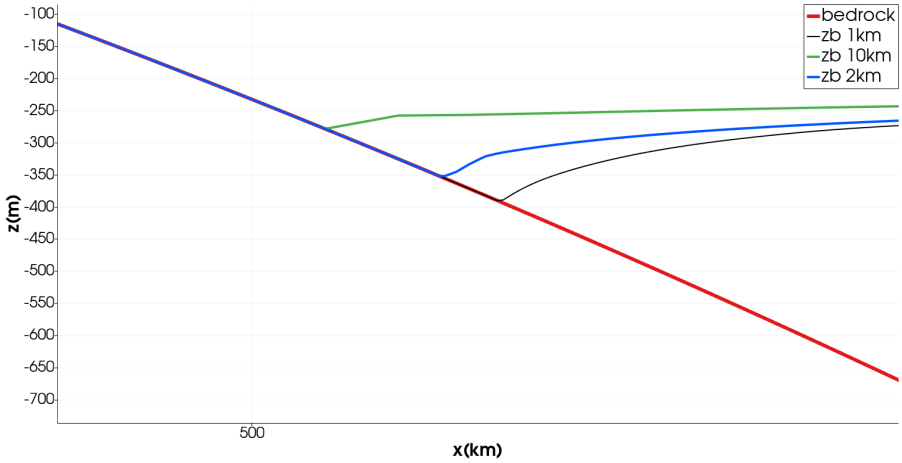

Figure 13: Position of the grounding line for different mesh resolutions.

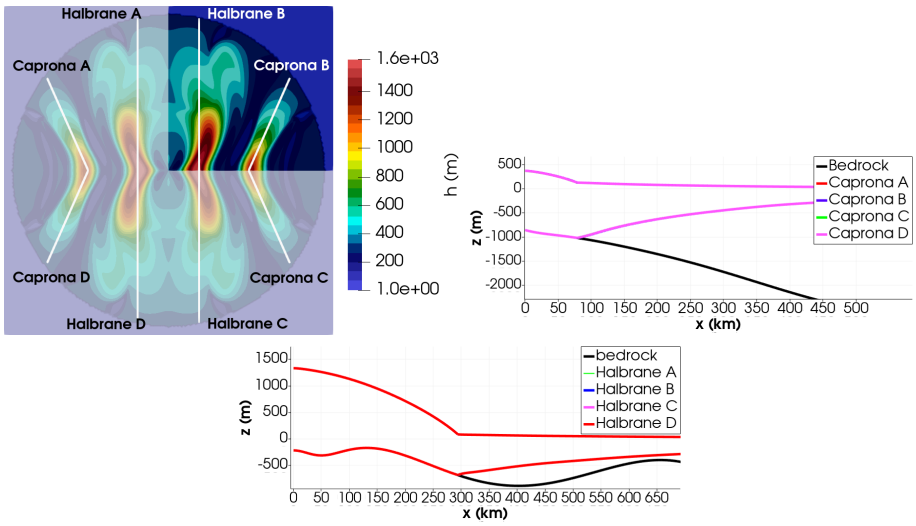

Figure 14: Profiles proposed for thule configuration. Highlighted the quarter of the domain

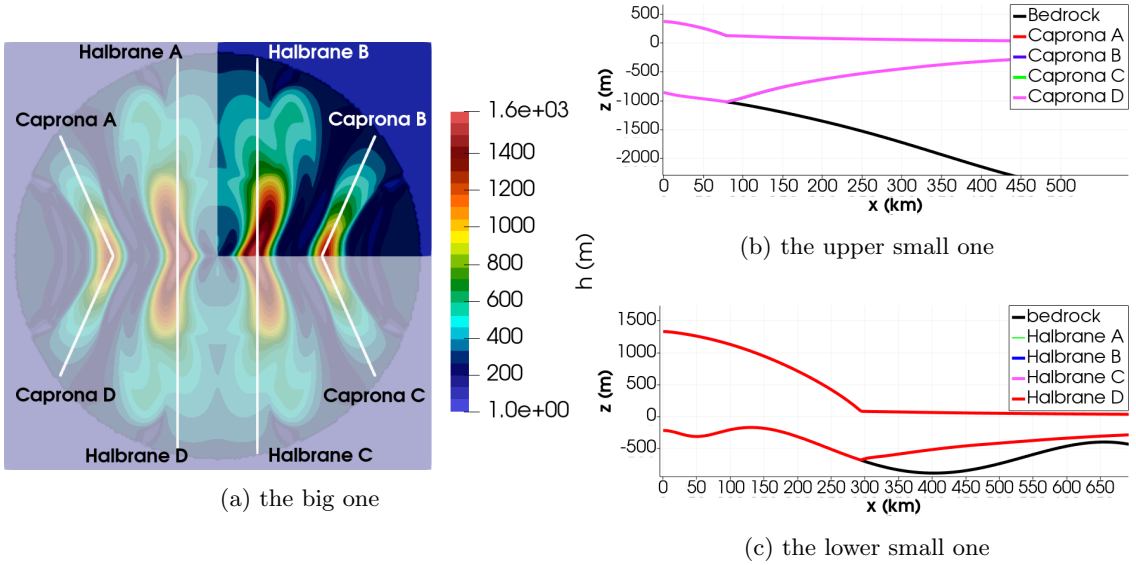

(a) the big one

(b) the upper small one

(c) the lower small one

Figure 15: The big caption for everyone

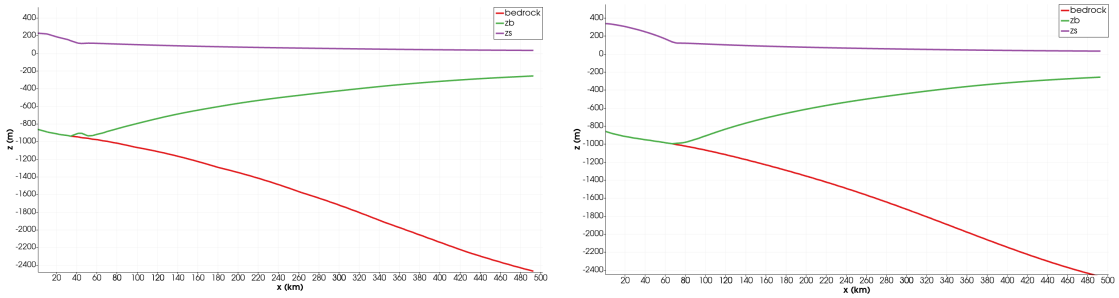

(a) 10km resolution result along Caprona B profile.

(b) 5km resolution result along Caprona B profile.

Figure 16: Plots of the ice sheet heights zb, zs and the position of the bedrock as a function of the horizontal position along Caprona B profile, for 10km and 5km resolution.

in figure 18.

Figure 19 shows a detailed plot of the comparison of the grounding line position along the Halbrane B profile for the different resolutions, where it can be identified as the position where zb and the bedrock start to be different, and the ice is no longer grounded.

4.3 Comparison with different constant parameters

Here we show the different results obtained with one complete domain for the previous constant parameters set up by the Calvin MIP project before the changes, which differences will be discussed in the next section.

5 Discussion

Here we will discuss the differences found between the results obtained for the different spacial resolutions for thule and cone, for the complete domain using the previous constant parameters, and the results obtained for the quarter domain using the new parameters. We will discuss the accuracy of the model for the different resolutions in predicting the position of the grounding line for both types of configurations. We will compare the position of the grounding line as a function of the resolution. Also, we will discuss the time spent in the simulations as a function of the number

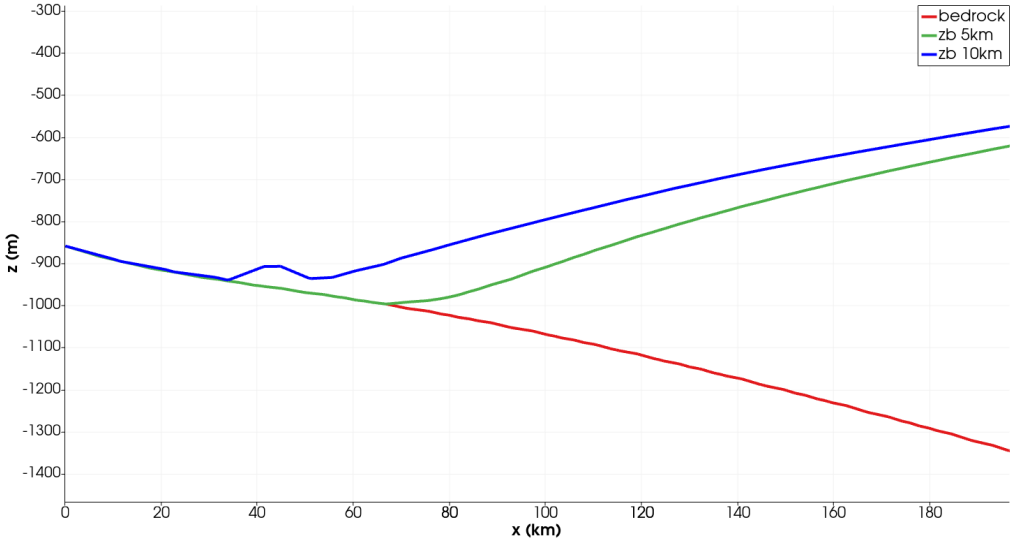

Figure 17: Grounding line position for different mesh resolutions along the Caprona B profile.

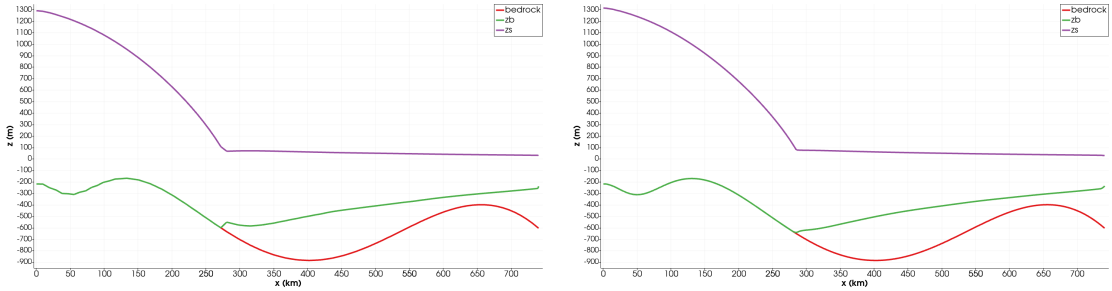

(a) 10km resolution result along Halbrane B profile. (b) 5km resolution result along Halbrane B profile.

Figure 18: Plots of the ice sheet heights zb, zs and the position of the bedrock as a function of the horizontal position along Halbrane B profile, for 10km and 5km resolution.

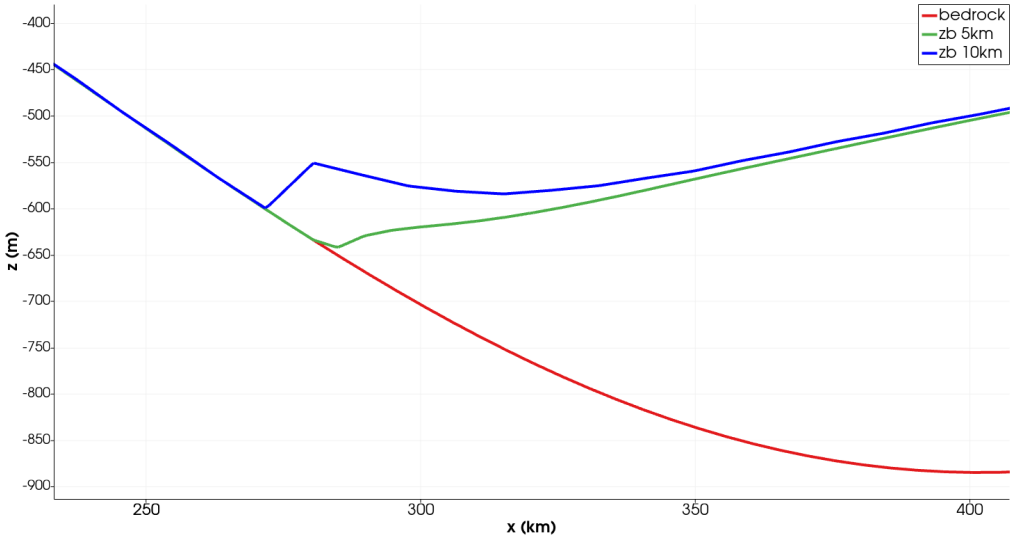

Figure 19: Grounding line position for different mesh resolutions along the Halbrane B profile.

of processors used (plot) and we can try to discuss an optimum number of processors that can be used (will be reviewed).

6 Conclusion

We will present our main conclusions of the project. The main objectives that were accomplished and future changes or improvements to do for further research.

References

[Allison et al., 2009] Allison, I., Alley, R., Fricker, H., Thomas, R., and Warner, R. (2009). Ice sheet mass balance and sea level. *Antarctic Science*, 21(5):413–426.

[Bamber et al., 2001] Bamber, J. L., Layberry, R. L., and Gogineni, S. (2001). A new ice thickness and bed data set for the greenland ice sheet: 1. measurement, data reduction, and errors. *Journal of Geophysical Research: Atmospheres*, 106(D24):33773–33780.

[Brunt et al., 2010] Brunt, K. M., Fricker, H. A., Padman, L., Scambos, T. A., and O'Neel, S. (2010). Mapping the grounding zone of the ross ice shelf, antarctica, using icesat laser altimetry. *Annals of Glaciology*, 51(55):71–79.

[Cheng et al., 2019] Cheng, G., Lötstedt, P., and von Sydow, L. (2019). A full stokes subgrid model for simulation of grounding line migration in ice sheets. *arXiv preprint arXiv:1908.10751*.

[Chugunov and Wilchinsky, 1996] Chugunov, V. A. and Wilchinsky, A. V. (1996). Modelling of a marine glacier and ice-sheet-ice-shelf transition zone based on asymptotic analysis. *Annals of Glaciology*, 23:59–67.

[Clark et al., 2015] Clark, P. U., Church, J. A., Gregory, J. M., and Payne, A. J. (2015). Recent progress in understanding and projecting regional and global mean sea level change. *Current Climate Change Reports*, 1(4):224–246.

[Courant et al., 1967] Courant, R., Friedrichs, K., and Lewy, H. (1967). On the partial difference equations of mathematical physics. *IBM journal of Research and Development*, 11(2):215–234.

[Durand et al., 2009a] Durand, G., Gagliardini, O., De Fleurian, B., Zwinger, T., and Le Meur, E. (2009a). Marine ice sheet dynamics: Hysteresis and neutral equilibrium. *Journal of Geophysical Research: Earth Surface*, 114(F3).

[Durand et al., 2009b] Durand, G., Gagliardini, O., Zwinger, T., Le Meur, E., and Hindmarsh, R. C. (2009b). Full stokes modeling of marine ice sheets: influence of the grid size. *Annals of Glaciology*, 50(52):109–114.

[Fricker et al., 2009] Fricker, H. A., Coleman, R., Padman, L., Scambos, T. A., Bohlander, J., and Brunt, K. M. (2009). Mapping the grounding zone of the amery ice shelf, east antarctica using insar, modis and icesat. *Antarctic Science*, 21(5):515–532.

[Friedl et al., 2020] Friedl, P., Weiser, F., Fluhrer, A., and Braun, M. H. (2020). Remote sensing of glacier and ice sheet grounding lines: A review. *Earth-Science Reviews*, 201:102948.

[Glen, 1958] Glen, J. (1958). The flow law of ice: A discussion of the assumptions made in glacier theory, their experimental foundations and consequences. *IASH Publ*, 47(171):e183.

[Goldberg et al., 2018] Goldberg, D., Snow, K., Holland, P., Jordan, J., Campin, J.-M., Heimbach, P., Arthern, R., and Jenkins, A. (2018). Representing grounding line migration in synchronous coupling between a marine ice sheet model and a z-coordinate ocean model. *Ocean Modelling*, 125:45–60.

[Haywood et al., 2011] Haywood, A., Dowsett, H. J., Robinson, M. M., Stoll, D. K., Dolan, A., Lunt, D., Otto-Bliesner, B., and Chandler, M. (2011). Pliocene model intercomparison project (pliomip): experimental design and boundary conditions (experiment 2). *Geoscientific Model Development*, 4(3):571–577.

[Hindmarsh, 1996] Hindmarsh, R. (1996). Stability of ice rises and uncoupled marine ice sheets. *Annals of Glaciology*, 23:105–115.

[Hutter, 1982] Hutter, K. (1982). A mathematical model of polythermal glaciers and ice sheets. *Geophysical & Astrophysical Fluid Dynamics*, 21(3-4):201–224.

[Konrad et al., 2018] Konrad, H., Shepherd, A., Gilbert, L., Hogg, A. E., McMillan, M., Muir, A., and Slater, T. (2018). Net retreat of antarctic glacier grounding lines. *Nature Geoscience*, 11(4):258–262.

[Larour et al., 2012] Larour, E., Seroussi, H., Morlighem, M., and Rignot, E. (2012). Continental scale, high order, high spatial resolution, ice sheet modeling using the ice sheet system model (issm). *Journal of Geophysical Research: Earth Surface*, 117(F1).

[MacAyeal, 1989] MacAyeal, D. R. (1989). Large-scale ice flow over a viscous basal sediment: Theory and application to ice stream b, antarctica. *Journal of Geophysical Research: Solid Earth*, 94(B4):4071–4087.

[Morlighem et al., 2017] Morlighem, M., Williams, C. N., Rignot, E., An, L., Arndt, J. E., Bamber, J. L., Catania, G., Chauché, N., Dowdeswell, J. A., Dorschel, B., et al. (2017). Bedmachine v3: Complete bed topography and ocean bathymetry mapping of greenland from multibeam echo sounding combined with mass conservation. *Geophysical research letters*, 44(21):11–051.

[Parizek and Walker, 2010] Parizek, B. R. and Walker, R. T. (2010). Implications of initial conditions and ice–ocean coupling for grounding-line evolution. *Earth and Planetary Science Letters*, 300(3-4):351–358.

[Pritchard et al., 2012] Pritchard, H., Ligtenberg, S. R., Fricker, H. A., Vaughan, D. G., van den Broeke, M. R., and Padman, L. (2012). Antarctic ice-sheet loss driven by basal melting of ice shelves. *Nature*, 484(7395):502–505.

[Schoof, 2007a] Schoof, C. (2007a). Ice sheet grounding line dynamics: Steady states, stability, and hysteresis. *Journal of Geophysical Research: Earth Surface*, 112(F3).

[Schoof, 2007b] Schoof, C. (2007b). Marine ice-sheet dynamics. part 1. the case of rapid sliding. *Journal of Fluid Mechanics*, 573:27–55.

[Van der Veen, 1985] Van der Veen, C. (1985). Response of a marine ice sheet to changes at the grounding line. *Quaternary Research*, 24(3):257–267.

[Vieli and Payne, 2005] Vieli, A. and Payne, A. J. (2005). Assessing the ability of numerical ice sheet models to simulate grounding line migration. *Journal of Geophysical Research: Earth Surface*, 110(F1).

[Weertman, 1974] Weertman, J. (1974). Stability of the junction of an ice sheet and an ice shelf. *Journal of Glaciology*, 13(67):3–11.

[Zhang et al., 2017] Zhang, T., Price, S., Ju, L., Leng, W., Brondex, J., Durand, G., and Gagliardini, O. (2017). A comparison of two stokes ice sheet models applied to the marine ice sheet model intercomparison project for plan view models (mismip3d). *The Cryosphere*, 11(1):179–190.